Interactions of the NADP(H)-Binding Domain III of Proton-Translocating Transhydrogenase from *Escherichia coli* with NADP(H) and the NAD(H)-Binding Domain I Studied by NMR and Site-Directed Mutagenesis†

Anders Bergkvist,*,‡ Carina Johansson,‡ Tomas Johansson,§ Jan Rydström,‡ and B. Göran Karlsson*,§

Department of Biochemistry and Biophysics, Göteborg University and Department of Molecular Biotechnology, Chalmers University of Technology, S-413 90 Göteborg, Sweden

Received February 22, 2000; Revised Manuscript Received June 27, 2000

ABSTRACT: Using the purified NADP(H)-binding domain of proton-translocating *Escherichia coli* transhydrogenase (ecIII) overexpressed in ^{15}N- and ^{2}H-labeled medium, together with the purified NAD(H)-binding domain from *E. coli* (ecI), the interface between ecIII and ecI, the NADP(H)-binding site and the influence on the interface by NAD(P)(H) was investigated in solution by NMR chemical shift mapping. Mapping of the NADP(H)-binding site showed that the NADP(H) substrate is bound to ecIII in an extended conformation at the C-terminal end of the parallel β-sheet. The distribution of chemical shift perturbations in the NADP(H)-binding site, and the nature of the interaction between ecI and ecIII, indicated that the nicotinamide moiety of NADP(H) is located near the loop comprising residues P346-G353, in agreement with the recently determined crystal structures of bovine [Prasad, G. S., et al. (1999) *Nat. Struct. Biol. 6*, 1126−1131] and human heart [White, A. W., et al. (2000) *Structure 8*, 1−12] transhydrogenases. Further chemical shift perturbation analysis also identified regions comprising residues G389-I406 and G430-V434 at the C-terminal end of ecIII's β-sheet as part of the ecI−ecIII interface, which were regulated by the redox state of the NAD(P)(H) substrates. To investigate the role of these loop regions in the interaction with domain I, the single cysteine mutants T393C, R425C, G430C, and A432C were generated in ecIII and the transhydrogenase activities of the resulting mutant proteins characterized using the NAD(H)-binding domain I from *Rhodospirillum rubrum* (rrI). All mutants except R425C showed altered NADP(H) binding and domain interaction properties. In contrast, the R425C mutant showed almost exclusively changes in the NADP(H)-binding properties, without changing the affinity for rrI. Finally, by combining the above conclusions with information obtained by a further characterization of previously constructed mutants, the implications of the findings were considered in a mechanistic context.

Nicotinamide nucleotide transhydrogenase (EC 1.6.1.1) is a membrane-bound enzyme that catalyzes a reversible reduction of $NADP^+$ by NADH coupled to a proton translocation across the cytoplasmic membrane:

$$H^+_{out} + NADP^+ + NADH \rightleftharpoons H^+_{in} + NADPH + NAD^+$$

Reduction of $NADP^+$ by NADH is denoted the forward reaction, and reduction of NAD^+ (or the analogue AcPyAD$^+$)[1] by NADPH is denoted the reverse reaction. Several different transhydrogenases have been cloned, and approximately 23% of the amino acids are invariant. The enzyme consists of three domains, domain I and III that bind NAD(H) and NADP(H), respectively, and the membrane-spanning domain II, through which protons are translocated. This organization is conserved between species (Figure 1), but the domains are distributed over one (e.g., bovine), two (e.g., *Escherichia coli*) or three (e.g., *Rhodospirillum rubrum*) polypeptide chains; a cyclic permutation is also found, e.g. in *Eimeria tenella* transhydrogenase. In *E. coli*, the α-subunit

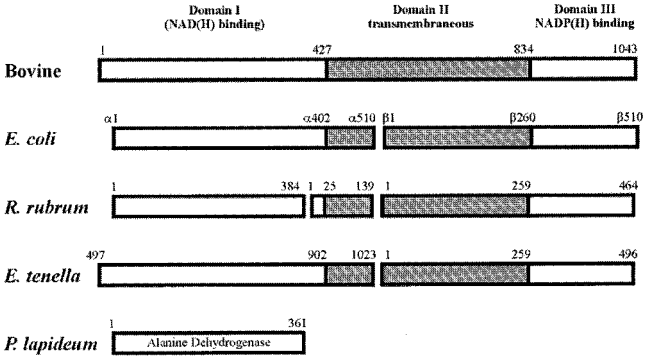

FIGURE 1: Domain organization of transhydrogenases. Alanine dehydrogenase is included for comparison. Soluble parts are shown as white boxes, and integral membrane domains are shaded.

† This work was supported by grants from the Swedish Natural Science Research Council and the Swedish Research Council for Engineering Sciences. C.J. acknowledges a grant from the Sven and Lilly Lawski Foundation.

* To whom correspondence should be addressed. E-mail: (B.G.K.) goran.karlsson@molbiotech.chalmers.se and (A.B.) anders.bergkvist@bcbp.gu.se. Fax: +46 31 7733910.

‡ Göteborg University.

§ Chalmers University of Technology.

[1] Abbreviations: dI, transhydrogenase domain I; dIII, transhydrogenase domain III; ecI, *E. coli* dI; ecIII, *E. coli* dIII; rrI, *R. rubrum* dI; rrIII, *R. rubrum* dIII; HSQC, heteronuclear single quantum coherence; AcPyAD$^+$, oxidised 3-acetylpyridine-NAD$^+$; AcPyADH, reduced 3-acetylpyridine-NADH.

10.1021/bi0004091 CCC: $19.00
Published on Web 09/23/2000

harbors the NAD(H)-binding domain, ecI, consisting of residues M1-S402, whereas the β-subunit harbors the NADP-(H)-binding domain, ecIII, consisting of residues C260-L462 (*1*−*4*).

The genes of the soluble domains of transhydrogenase from several species have been overexpressed and the proteins have been purified and characterized (*5*−*9*). In all cases, domain I was expressed as a dimer and found to lack bound substrates. In contrast, isolated domain III exists as a monomer and contains tightly bound NADP(H), reflecting a dramatically increased affinity for NADP(H) as compared to the intact enzyme. Even in the absence of the transmembrane domain II, domain I and III from the same or different species form a catalytically active complex capable of catalyzing the various transhydrogenation reactions (*6*−*8*, *10*). However, the tight binding of NADP(H) and thus the limiting NADP(H) release results in low reaction rates for the reverse and forward reactions catalyzed by the dI·dIII complex (*7*, *10*−*13*).

In *R. rubrum*, rrI is naturally expressed as a separate soluble subunit. The rrI·rrIII and rrI·ecIII complexes catalyze a cyclic reaction, i.e., reduction of the NAD-analogue $AcPyAD^+$ by NADH mediated by bound NADP(H) in domain III, essentially with the same characteristics and rates as those of the intact *R. rubrum* enzyme (*7*, *10*). The rrI·rrIII or rrI·ecIII complexes could thus be regarded as nearly identical to the intact enzyme during hydride transfer. In contrast, a mixture of ecI + ecIII catalyzes hydride transfer only at a very low rate (*5*), which may be explained by a low affinity between the two *E. coli* domains in solution making the complex short-lived (*10*). The different properties of the ecI·ecIII and the rrI·ecIII complexes have proven very useful. Utilizing the short-lived ecI·ecIII complex made it possible to measure chemical shift changes with fast exchange in NMR, whereas the more long-lived rrI·ecIII proved suitable for performing kinetic assays at reliably measurable reaction rates.

Until recently the structural information available for the soluble domains of transhydrogenase has been scarce. A predicted model of ecI was presented which was suggested to contain a classical dinucleotide-binding domain similar to that in alanine dehydrogenase (*14*). A global fold and identification of the substrate-binding site of ecIII, based on NMR data, has also been presented (*15*). However, only limited information is available regarding the structural aspects of complex formation between the two hydrophilic transhydrogenase domains (*16*). Recently, however, high-resolution crystal structures of domain III of bovine (*17*) and human (*18*, *19*) heart transhydrogenases, both with bound $NADP^+$, have been presented. The structural information essentially confirmed the global fold concluded earlier (*15*) although at a molecular level. Moreover, as previously considered a possibility (*20*), the positioning of the bound $NADP^+$ was shown to be turned 180° as compared to most other dehydrogenases/reductases (*17*, *19*).

By using NMR in combination with mutagenesis, an extensive characterization of the interface between ecIII and ecI, as well as a characterization of the NADP(H)-binding site and structural changes in ecIII following NAD(H) binding in ecI, has been carried out. In addition to information regarding important residues involved in the NADP(H)-binding site and the ecI−ecIII interface, the results reveal unexpected redox-dependent changes of the ecI−ecIII interface suggested to be relevant for the overall reaction mechanism of the intact enzyme.

MATERIALS AND METHODS

Site-Directed Mutagenesis. Cysteine mutations were introduced into the ecIII gene at positions T393, R425, G430, and A432. All mutants except R425C were constructed using the pET8c plasmid (*5*) carrying the ecIII gene as a DNA template. The R425C mutant was based on the pEcIII plasmid, in which the ecIII gene is under control of a lac promoter (*20*). The mutants were introduced by using the Quikchange mutagenesis kit (Stratagene) as described by the manufacturer. The correctness of the mutant products was checked by DNA sequencing.

Expression and Purification. Wild-type and mutant ecIII were derived from the C-terminal 177 residues (βD285-βL462) of the *E. coli* transhydrogenase β-subunit. The R425C mutant plasmid was transformed into *E. coli* TG1 cells and expressed as described in ref *20*, while the wild-type and other mutant plasmids were transformed into *E. coli* BL21(DE3) cells and expressed as described in ref *5*. All ecIII genes were expressed with an N-terminal His-tag. The purification of the wild-type and mutant ecIII domains was carried out essentially as described in ref *5*, except that the domains were eluted from the gel filtration column in 10 mM sodium phosphate buffer (pH 7.0) containing 100 mM NaCl. The wild-type protein was uniformly ^{15}N-labeled and 85% ^2H-labeled by growing the cells in 99% D_2O and using $^{15}NH_4Cl$ (Martek) as the sole nitrogen source in M9 medium. Carbon-labeled wild-type protein was prepared by growing cells in [^{13}C]glucose as the sole carbon source. Following purification, integrity of the protein and level of labeling were checked with MALDI-TOF mass spectroscopy.

The NAD(H)-binding N-terminal 394 residues of the *E. coli* transhydrogenase α-subunit (ecI) were subcloned following an N-terminal Met-$(His)_6$-Gly tag and expressed in TG1 cells under the control of the *lac* promoter (*5*). The cells were grown in LB-medium at 37 °C for about 18 h, after which they were harvested at 7000 rpm for 15 min at a temperature of 4 °C, frozen, and stored at −80 °C. The methods used for further purification of ecI were the same as those for ecIII.

A plasmid, pCD1, containing the gene coding for rrI, was transformed into the TG1 strain of *E. coli*. The gene was overexpressed (*6*), and the protein purified following the method described (*21*) with modifications. The supernatant obtained after sonication and centrifugation of 1 L of culture was loaded onto a 15 mL Q-Sepharose HP column (Pharmacia) equilibrated with 20 mM Tris-HCl and 10 mM $(NH_4)_2SO_4$ (pH 8.0). The protein was eluted with about 70 mL of the same buffer. $(NH_4)_2SO_4$ was then added to the sample to a concentration of 1.6 M. After 1 h incubation the sample was centrifuged for 1 h at 18 000 rpm in a Beckman JA20 rotor, and the supernatant was loaded onto a 20 mL Butyl Toyopearl column (Tosohaas). The protein was eluted with a gradient (300 mL) of 1.6 to 0 M $(NH_4)_2SO_4$ in 20 mM Tris-HCl (pH 8.0), and stored at −20 °C in 20% glycerol.

All domains displayed a purity greater than 90% as judged by SDS−polyacrylamide gel electrophoresis using 8−25%

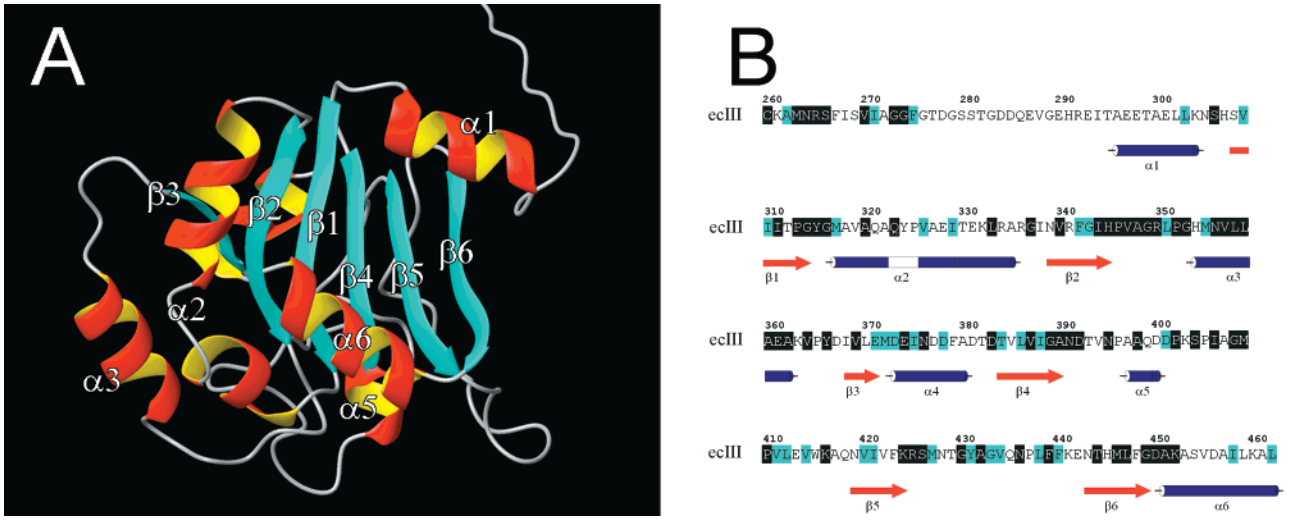

FIGURE 2: Solution structure model and secondary structure elements of ecIII based on NMR data. (A) Solution structure model of ecIII. The parallel β-sheet, comprising β-strands 3, 2, 1, 4, 5, and 6, is visible in the center of the protein. α-helices 3, 2, 6, and 1 are facing the viewer and α-helix 4 and loops between β4 and β5 and between β5 and β6 are situated behind the β-sheet. (B) Amino acid sequence with secondary structure elements of ecIII. Black shaded residues are conserved and gray shaded residues are similar among different species of transhydrogenase.

gradient gels in the Phast system (Amersham Pharmacia Biotech).

Determination of Protein Concentration and Substrate Content. Protein concentrations were determined by absorbance spectroscopy at 280 nm, using $\epsilon_{ecIII(NADP+)} = 15\,000$ M^{-1} cm^{-1} and $\epsilon_{ecI(apo)} = 23\,470$ M^{-1} cm^{-1}. Alternatively, the bicinchoninic acid assay with bovine serum albumin as standard was used for protein determination (*22*).

Substrate binding was determined by UV−vis spectroscopy. The theoretical ϵ_{280} is 10 800 M^{-1} cm^{-1}, whereas ϵ_{260} of the $NADP^+$ substrate is 18 000 M^{-1} cm^{-1}; λ_{max} is therefore a good indicator of the fraction of apo-protein. The absorbance at 340 nm was used to determine the redox state of the substrate, whereas the content of $NADP^+$ in wild-type and mutant ecIII was determined by fluorescence using a modified Klingenberg procedure as described previously (*5*).

Activity Assays. Transhydrogenation reactions catalyzed by mutant and wild-type ecIII were analyzed using *R. rubrum* domain I. Protein−protein titrations were performed in which the ecIII concentration was kept constant, and the rrI concentration was varied until a maximum rate was achieved. The dI·dIII assay buffer [20 mM each of Mes, Mops, Ches, and Tris, 50 mM NaCl (pH 7.0)] was used for assay of this reconstituted dI·dIII system. The reverse and cyclic reactions were measured optically as described (*5*, *23*). Measurements were performed at 25 °C.

NMR Experiments. NMR samples contained 0.9−1.5 mM ecIII in 10 mM sodium phosphate, 100 mM NaCl, and 90% H_2O/10% D_2O at pH 7.0, and experiments were performed at 25 °C on Varian Inova spectrometers. The backbone assignment of ecIII has been reported earlier (*24*). Side chain and NOE assignments were accomplished using a number of heteronuclear NMR experiments. ^{15}N-filtered NOESY−HSQC spectra were recorded at 600 and 800 MHz with mixing times between 50 and 200 ms. ^{15}N-filtered TOCSY−HSQC experiments were performed at 600 MHz with a mixing time of 50 ms. A HCCH-TOCSY and a ^{13}C NOESY−HSQC experiment were performed at 800 MHz using mixing times of 21 and 50 ms, respectively.

^{15}N and H^N chemical shift changes in ecIII upon alterations in domain interaction and substrate-binding states were monitored in ^{15}N HSQC spectra at 800 MHz. These spectra were recorded with 2048 complex points in t_2 and 512 t_1 increments, with sweep widths of 12 000 and 3003 Hz, respectively. Data in the indirect dimension were zero-filled to twice the amount of acquired points and apodized using a Gaussian window function before Fourier transformation. NMR data were analyzed using ANSIG (*25*, *26*).

Solution Structure Model Determination. A solution structure model of ecIII (Figure 2) was obtained by applying 102 H^N-H^N NOEs, 64 additional NOEs involving side chain protons, 67 dihedral angles and 42 × 2 hydrogen bonds as restraints in a structure calculation using the standard annealing protocol in DYANA (*27*). The NOEs were classified according to the following scheme. H^N to H^N sequential NOEs were given an upper limit of 3.0 Å, α-helical H^N to H^N (i,i+2) were given an upper limit of 4.5 Å and long-range H^N-H^N NOEs were given upper limits of 3.1, 4.0, or 5.0 Å based on NOE intensity. H^N to H^α sequential NOEs occurring in β-strands were given upper limits of 2.5 Å and the upper limit of NOEs involving methyl groups was set to 5.0 Å. The dihedral angles were introduced based on chemical shift information and subsequent secondary structure identification as ψ angle restraint intervals of 110−180° for β-strands and −55 to −15° for α-helices. The hydrogen bonds were introduced as distance restraint intervals, 2.0−1.8 Å between the amide proton and the acceptor atom and 3.0−2.7 Å between the amide nitrogen and the acceptor atom, based on amide exchange information, when the acceptor atom could be identified in regular secondary structure elements. An ensemble of 20 structures was calculated and 10 of these structures with the lowest overall target function were selected for further analysis.

Domain and Substrate Titrations for NMR. A stock solution of 1.1 mM apo-ecI was prepared in a 10 mM sodium phosphate, 100 mM NaCl, and 90% H_2O/10% D_2O buffer at pH 7.0. At the titration steps, amounts from this stock solution were added to and mixed with a NMR sample of

Table 1: Content of Bound NADP(H) in Wild-Type and Mutant ecIII[a]

ecIII enzyme	λ_{max}	$NADP^+$ (%)	NADPH (%)	apo-form (%)	ref
ecIII	267	87	5	8	this study
ecIIIH345C	267	44	25	31	*20*
ecIIIA348C	267	6	60	34	*20*
ecIIIR350C	267	24	30	46	*20*
ecIIID392C	277	0	0	100	*20*
ecIIIT393C	267	34	66	0	this study
ecIIIK424C	267	22	15	63	*20*
ecIIIR425C	277	0	0	100	this study
ecIIIG430C	267	3	65	32	this study
ecIIIA432C	267	0	78	22	this study

[a] The concentrations of NADPH were estimated from UV−vis spectra and the concentrations of $NADP^+$ were determined by a modified Klingenberg procedure (See Materials and Methods). The λ_{max} value corresponds to the wavelength at which maximal absorption was observed for the interval 230−450 nm in UV−vis spectra.

0.9 mM ecIII at molar ecI:ecIII ratios of 0, 1, and 2. After each addition of ecI, the NMR sample was concentrated in order to maintain the ecIII concentration. The pH of the protein solution was checked before each measurement and was, when necessary, adjusted to 7.0. After the last NMR experiment in the titration series, the sample with an ecI:ecIII molar ratio of 2 was supplemented first with NAD^+ and then with NADH. Substrates were taken from concentrated stock solutions and reached final concentrations of 4 mM each in the NMR sample. Since the added volumes of substrates were small, the dilution effects were considered negligible.

To visualize the chemical shift differences between the different forms of ecIII, the solution structure model was color coded according to the magnitude of chemical shift perturbation in each residue. Residues were considered strongly perturbed if the magnitude of perturbation for either H^N or ^{15}N exceeded 32 or 12 Hz, respectively, and colored red. Residues whose magnitude of perturbation for H^N or ^{15}N were in the interval 16−32 Hz or 6−12 Hz, respectively, were colored yellow. Residues whose amide pair had not been assigned, were overlapped, were too weak to be observed or for other reasons could not be accurately observed in the ^{15}N−HSQC spectra were colored pale green. Observable residues with chemical shift changes below 16 Hz (H^N) and 6 Hz (^{15}N), were colored white. Color illustrations were prepared using MOLMOL (*28*).

RESULTS

Expression and Purification of ecIII. Expression levels using M9 minimal medium yielded approximately 13 mg of deuterated ^{15}N-labeled wild-type ecIII/L of culture, a higher yield than previously reported (*15*). EcIII behaved as a monomer both in light scattering and size-exclusion chromatography experiments (data not shown).

A set of cysteine mutants, i.e., T393C, R425C, G430C, and A432C were constructed and characterized in which conserved or semi-conserved residues were targeted based on loop regions in the protein which were predicted to be exposed on the surface (*20*) (Table 1). Additional, but previously constructed mutants included in this investigation were H345C, A348C, R350C, and D392C (*20*) (Table 1). All were cysteine residues since they will be reacted with thiol-specific probes in a forthcoming study. However, in the present investigation the mutants were used as local perturbations at the respective sites of the protein. The yield of mutant ecIII varied between 1 to 15 mg of protein/L of cultivation. Interestingly, the G430C mutant spontaneously formed dimers during purification. The existence of disulfide bridges was corroborated by running SDS−PAGE in the presence and absence of a reducing agent (not shown).

One of the characteristic features of the separately expressed wild-type ecIII domain was its content of tightly bound NADP(H) in almost 100% of the protein molecules (*5*). The proportion of oxidized and reduced bound substrate varied less than 5% from one preparation to another for the same wild-type or mutant protein. To examine if a mutation affected these substrate-binding properties, λ_{max} and the proportions of NADPH and $NADP^+$ were routinely determined in all mutants. Table 1 summarizes the results for the ecIII mutants constructed in this work and also lists a comparison with previously characterized ecIII mutants. It can be noted that in all mutants, except for T393C, in which case the apo-form was absent, the proportion of apo-protein was increased reflecting a lowered substrate affinity than that of the wild-type ecIII. The NADPH/$NADP^+$ ratio was also changed, especially when a mutation was introduced in loops succeeding β3, β4, and β5 (cf. Figure 2), i.e., in the case of A348C, T393C, G430C, and A432C, in which case this ratio was inverted. The most dramatic change, however, occurred in the D392C and R425C mutants, which both were devoid of bound substrate and thus displayed a λ_{max} at 277 nm. This suggests that these two residues are crucial for substrate binding.

Expression and Purification of ecI and rrI. The yield of ecI was approximately 42 mg/L whereas that of rrI was approximately 100 mg/L. UV−vis spectroscopy suggested that both ecI and rrI were purified in the apo-form. Size-exclusion chromatography showed that both ecI and rrI migrate as dimers, in agreement with earlier findings (*5*, *6*).

NMR Experiments. A rotational correlation time of 14 ns for ecIII (*15*, *24*) constitutes an unusually unfavorable condition for NMR experiments and a deuterated sample was therefore required. The 2D ^{15}N HSQC spectrum of 85% deuterated ^{15}N-labeled isolated ecIII exhibited an excellent signal dispersion and 213 peaks were readily identified (Figure 3). EcIII was expected to give rise to 175 backbone signals, 72 side-chain signals, and 4 signals from the bound substrate, in total 251 possibly observable signals. The previously reported backbone assignment (*24*), included all amide proton and nitrogen resonances with the exception for the His-tag and three residues in the unstructured N-terminus. Of these signals, 14 were overlapped or exchange broadened, thus allowing the assignment and monitoring of up to 150 signals in the subsequent interaction analysis.

Solution Structure Model. Ten structures with the lowest overall target functions were selected from 20 calculated structures in DYANA. The average global RMSD between the regular secondary structure elements of these 10 structures were 4.5 ± 1.0 Å (Table 2).

One of the 10 structures was selected as a model for the global fold (Figure 2). A large number of H^N-H^N NOEs between the β-strands unambiguously defined a central parallel β-sheet with the strand order 3, 2, 1, 4, 5, and 6.

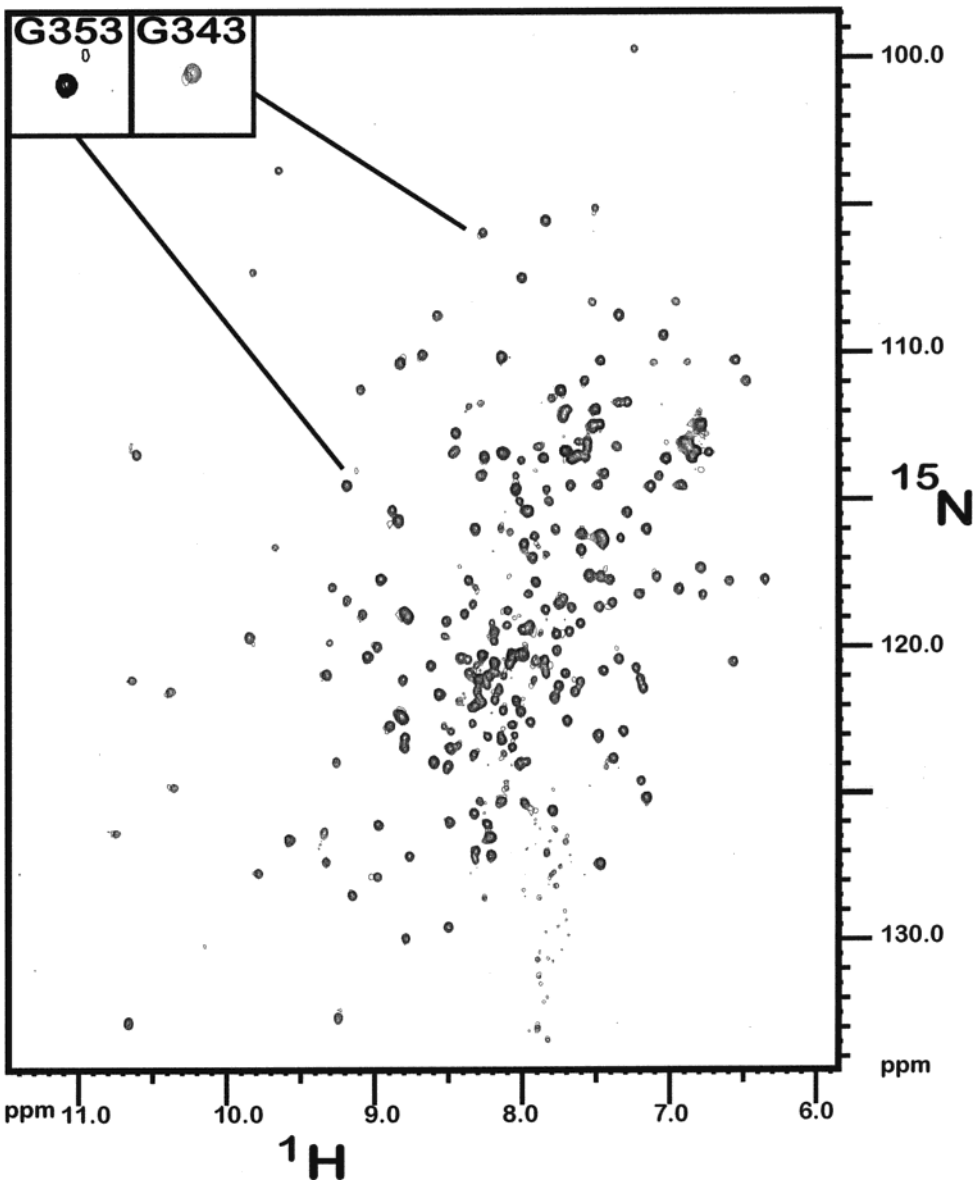

FIGURE 3: ^{15}N−HSQC spectra of isolated ecIII(NADP$^+$) and of ecIII(NADP$^+$)·ecI(apo) showing chemical shift perturbations upon complex formation between ecIII and ecI. Boxed peaks highlight examples of amide groups that shift upon complex formation. G353 is an example of a peak which shifted more than 32 Hz in the H^N-dimension or more than 12 Hz in the ^{15}N-dimension (colored red in subsequent figures). G343 is an example of a peak which shifted in the intervals 16−32 Hz in the H^N-dimension or 6−12 Hz in the ^{15}N-dimension (colored yellow in subsequent figures).

This type of β-sheet introduces sterical restrictions on the α-helices and loops around the β-sheet. Specifically, helix α2 and α3 were topologically confined to different sides of the β-sheet than α4 and α5 which was confirmed by several NOEs. A folding motif with such a β-sheet and arrangement of α-helices is typical of a classical dinucleotide-binding motif. Long-range NOEs defined the positions of α1 and α6 on the same side as α2 and α3. Interestingly, α1 and α6 arranged themselves diagonally across the β-sheet with the C-terminal end of α6, i.e., the C-terminus of the protein, almost buried in the center of the protein next to α2. The secondary structures between β4 and β5 and between β5 and β6 were largely comprised of loops and few long-range NOEs were assigned to these regions. Nevertheless, sterical interferences prevented these elements from occurring on the same side as α1 and α6.

Chemical Shift Perturbation Mapping. Upon addition of ecI(apo) to ecIII(NADP$^+$), chemical shift perturbations were

Table 2: Statistics for ecIII Global Fold Structure Calculation[a]

structure generation	
restraint type	number
NOEs, total	166
sequential ($\|i - j\| = 1$)	65
medium range ($1 < \|i - j\| < 5$)	38
long range ($\|i - j\| \geq 5$)	63
dihedral angles	67
hydrogen bonds	84
structure evaluation	
average global RMSD	4.5 ± 1.0 Å

[a] The dihedral angle restraints were included as ψ angles based on a chemical shift index calculation. Hydrogen bonds were included as two distance restraints based on deuterium exchange experiments, one from the slowly exchanging proton to the acceptor atom and one from the donor to the acceptor atom. The structure evaluation was performed on an ensemble of 10 nonedited structures. The average global RMSD was evaluated on the regular secondary structure elements as listed in Figure 3B.

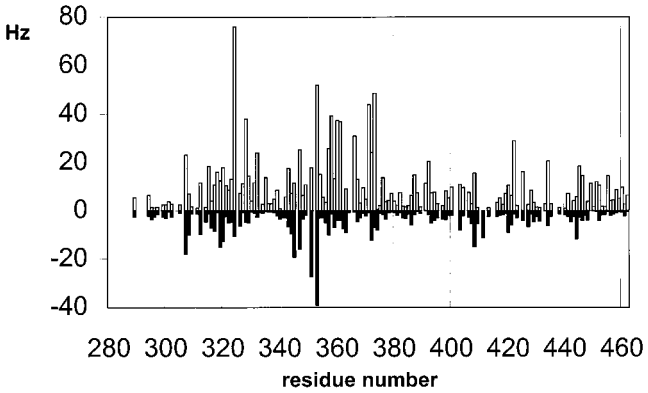

FIGURE 4: Chemical shift differences from ^{15}N−HSQC peaks between isolated ecIII(NADP$^+$) and the ecIII(NADP$^+$)·ecI(apo) complex. The ecI/ecIII ratio was 1:2. Open bars correspond to the amplitude of ^{1}H and filled bars correspond to the negative amplitude of ^{15}N chemical shift perturbations, respectively.

detected in the ^{15}N−HSQC spectra (Figure 3). The interaction was governed by fast exchange, and chemical shift changes were traced in a series of titrations. The chemical shift changes between isolated ecIII(NADP$^+$) and ecIII(NADP$^+$) in complex with ecI(apo) at an ecI/ecIII molar ratio of 2 are shown in Figure 4. At the protein concentrations used, the ecI·ecIII complex could not be saturated with ecI, and the complex lifetime could therefore not be determined. However, the largest fast-exchanging chemical shift perturbation at a ecI/ecIII molar ratio of 2, i.e., 76.0 Hz (the amide proton of residue Y324) on the 800 MHz spectrometer, corresponded to an upper limit of the complex lifetime (*29*) of 14 ms. For comparative reasons, ecIII(NADP$^+$) was mixed with rrI(apo) and analyzed in an ^{15}N−HSQC spectrum. Due to the long lifetime of the resulting complex most of the resonance signals were in slow exchange and the interaction could not be followed as chemical shift changes. However, several resonances showed exchange broadening, indicating that they were involved in the ecIII(NADP$^+$)·rrI(apo) interface and that the corresponding residues were qualitatively the same as those found in the ecIII(NADP$^+$) + ecI(apo) titration series (results not shown). Quirk et al. (*16*) reported exchange broadening in the corresponding rrIII(NADP$^+$)·rrI(apo) complex. The implicated residues agree with our findings, even though the two structural NMR models differ cf. (*15*, *16*).

Chemical shifts of individual residues are depicted as strong (red), intermediate (yellow), and no observed changes (white/green) (Figure 5) as described in Materials and Methods. The chemical shift changes of the H^N and the ^{15}N

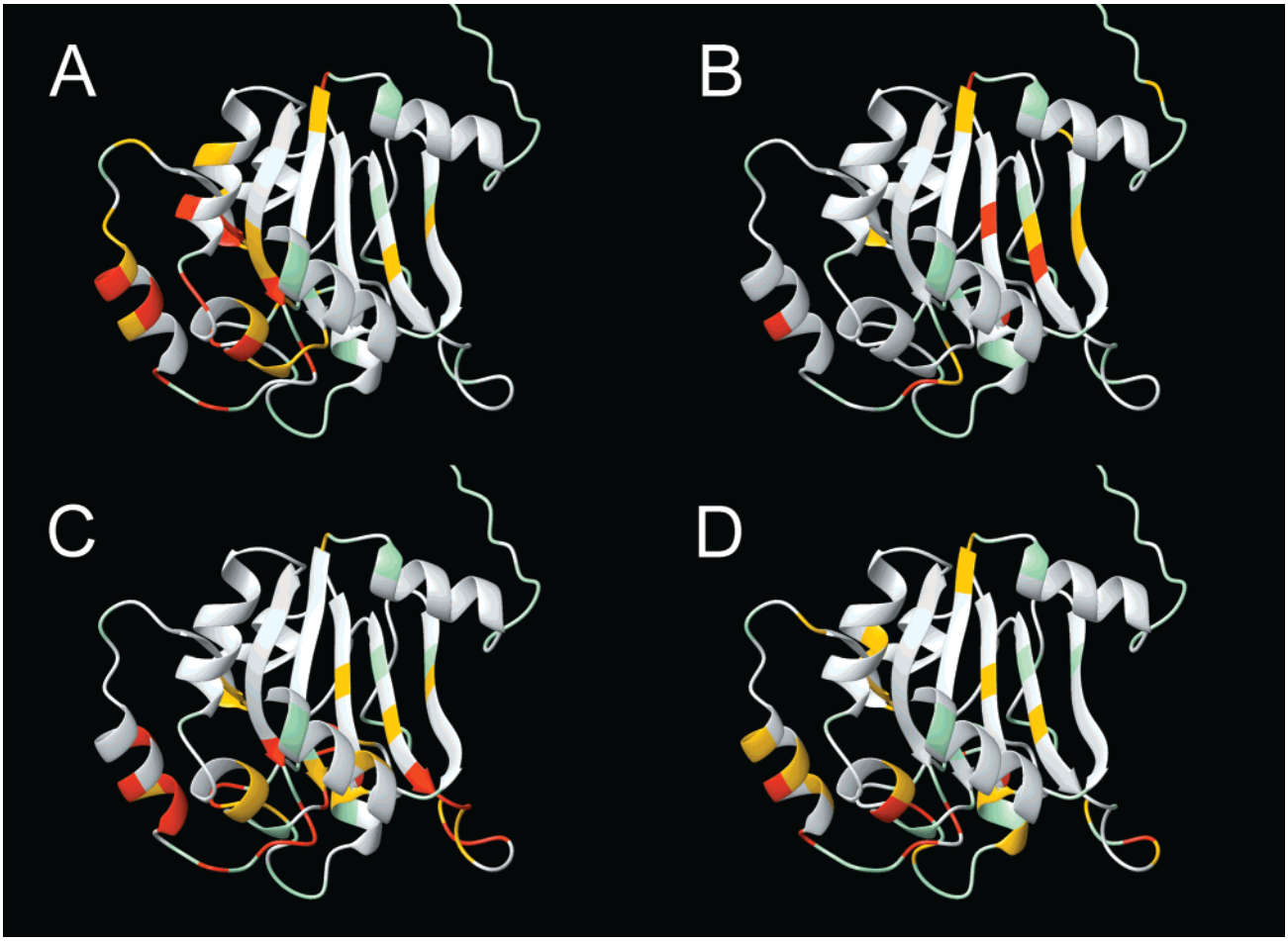

FIGURE 5: Color-coded solution structure models demonstrating the chemical shift differences between various complexed or isolated forms of ecIII. (A) ecIII(NADP$^+$) compared to ecIII(NADP$^+$)·ecI(apo). (B) ecIII(NADP$^+$)·ecI(apo) compared to ecIII(NADP$^+$)·ecI(NAD$^+$). (C) ecIII(NADP$^+$) compared to ecIII(NADPH). (D) {ecIII(NADPH)·ecI(NADH) − ecIII(NADPH)} − {ecIII(NADP$^+$)·ecI(NAD$^+$) − ecIII(NADP$^+$)}. Residues with no or small chemical shift perturbations are colored white. Chemical shift differences larger than 16 (H^N) or 6 (^{15}N) Hz, but not larger than 32 (H^N) or 12 (^{15}N) Hz, are colored yellow. Chemical shift differences larger than 32 (H^N) or 12 (^{15}N) Hz are colored red. Residues that are exchange broadened below the limit of detection, shifted beyond detection, overlapped or lacking assignments are colored pale green.

nuclei were thus compiled and color-coding was performed on a per-residue basis. However, interpretations of the chemical shift changes (see below) were performed with emphasis on regions rather than on individual residues.

A color-coded solution structure model illustrating the chemical shift differences between the isolated ecIII and the ecI complex form of ecIII is shown in Figure 5A. The largest chemical shift differences occurred in α2 (V319−E328), in the loop connecting *β*2 with α3 (G343−G353), in α3 (L358−E361), and at the N-terminal end of α4 (E371−E374). Local chemical shift changes also occurred at the center of *β*5 (V422) and *β*6 (H445), and around the N-terminal end of *β*1 (H307−S308). Some chemical shift changes were also observed in the loops between *β*4 and *β*5 (D392, G408, V411) and between *β*5 and *β*6 (V434). No chemical shift changes were observed in α1 and α6.

To investigate the effects of NAD(H) binding in ecI on ecIII, NAD^+ was first added to the ecIII($NADP^+$)·ecI(apo) NMR sample. The ^{15}N−HSQC spectrum of ecIII($NADP^+$) in complex with ecI(NAD^+) showed significant chemical shift differences as compared to that of the ecIII($NADP^+$)·ecI(apo) complex (Figure 5B). As a consequence of NAD^+ binding to ecI, chemical shift changes were detected in the loop connecting *β*2 and α3 (V347−G349) and in α3 (V357). Significant chemical shift changes were also observed in the part of the *β*-sheet formed by *β*4 (L386, G389), *β*5 (I421, V422), and *β*6 (H445, M446). With the exception of the N-terminal end of *β*1, chemical shift changes were not observed in the other *β*-strands, α1, α6, or the loops between *β*4 and *β*5 and between *β*5 and *β*6.

A change of the redox state of NADP(H) also affected the chemical shifts of ecIII (*15*) and rrIII (*16*). Previous qualitative results have shown that the chemical shift differences between isolated ecIII($NADP^+$) and isolated ecIII(NADPH) map out the C-terminal end of the *β*-sheet (*15*), the expected substrate-binding site in a dinucleotide-binding motif. The available structure model and a more quantitative analysis made it possible to map the chemical shift perturbations on the structure model caused by exchange of $NADP^+$ for NADPH (Figure 5C). It is clear that the C-terminal end of the protein constitutes the substrate-binding site. The fact that chemical shift perturbations occur across the length of the *β*-sheet indicates that the substrate is bound in an extended conformation. Several strong chemical shift perturbations occurred in the loop connecting *β*2 and α3 (H345−L351), and in α3 itself (H354−L359) upon addition of NADPH. These results indicate that, in agreement with the crystal structures of the mitochondrial domain III (*17*, *19*), the nicotinamide moiety in NADP(H) is located near the loop connecting *β*2 and α3 (residues P346−G353) in ecIII. The loops following *β*4 (G389−A397, I406−M409) and *β*5 (K424−V434) showed significant chemical shift changes, indicating that these regions are important for substrate affinity and/or specificity.

A substrate redox change can also be achieved in the ecIII($NADP^+$)·ecI(NAD^+) complex by the addition of NADH. Since the affinities of rrI/ecIII and ecIII for the reduced substrates are much greater than those for the oxidized equivalents (*5*, *30*), addition of NADH will rapidly replace NAD^+ in rrI and reduce $NADP^+$ to NADPH in ecIII. Evaluating the chemical shift differences between the resulting ecIII(NADPH)·ecI(NADH) complex and isolated ecIII(NADPH) gives the interaction surface of ecIII with ecI in the presence of reduced substrates. In the same manner, the interaction surface obtained with oxidized substrates was derived by evaluating the chemical shift differences between the ecIII($NADP^+$)·ecI(NAD^+) complex and isolated ecIII($NADP^+$). Chemical shift mapping of both these interaction surfaces showed large similarities with that in the ecIII($NADP^+$)·ecI(apo) complex (Figure 5A). However, the difference between the two interaction surfaces may be evaluated in order to deduce changes as a result of redox change of the substrates, i.e., {ecIII(NADPH)·ecI(NADH) − ecIII(NADPH)} − {ecIII($NADP^+$)·ecI(NAD^+) − ecIII($NADP^+$)}. The resulting chemical shift perturbations were mapped on the structure model in Figure 5D. Once again, chemical shift perturbations in α2 (V319, A320, T330), in the loop connecting *β*2 and α3 (V347−G353) and in α3 (M355−E361) were observed. However, this time perturbations in the loops between *β*4 and *β*5 (G389−I406) and between *β*5 and *β*6 (G430−V434) were also observed. These perturbations were particularly interesting since the previous domain interaction studies (Figure 5A) showed no indication that these residues participate in the interaction surface of ecIII with ecI. The perturbations thus suggest that these regions are in redox-regulated contact with ecI or that they are indirectly affected through the substrate-binding site. In either case, the regions identified here seem to have important roles in the mechanism of action of the protein.

Substrate Binding and Catalytic Activities of Mutants. Of the mutated residues used in this investigation, residues H345, A348, and R350 are located in the loop between *β*2 and α3, residues D392 and T393 are located in the loop following *β*4 and residues K424, R425, G430, and A432 are located in the loop following *β*5. All of these residues are believed to form part of the interface and/or the NADP(H)-binding site (*17*−*20*) and also show chemical shift perturbations in the present NMR study. The reverse and cyclic reactions catalyzed by mutant ecIII + rrI mixtures were analyzed using protein−protein titrations in which the ecIII concentration was kept constant and rrI varied until a maximal reaction rate was reached, giving a [rrI]/[ecIII] ratio required for half-saturation.

The maximal rate of the reverse reaction catalyzed by mixtures of rrI and ecIII at pH 7.0 has been shown to be limited by the slow release of $NADP^+$ (*7*, *10*−*13*). All cysteine mutants described in Table 3 showed increased maximal reverse rates, which in most cases is explained by the decreased affinity for NADP(H) caused by the introduced mutation (cf. Table 1). Thus, mutation of the neighboring residues D392 and T393 to cysteines led to completely opposite effects with respect to content of NADP(H), i.e., the former showed 100% apo-form whereas the latter showed 0% apo-form (Table 1). Consequently, the D392C mutant catalyzed the highest reverse activity and T393C one of the lowest activities (Table 3). K424C, R350C, H345C, and A432C showed an almost linear correlation between content of apo-form and activity, whereas A348C and G430C both had an NADP(H) content of 32−34% and an unproportionately high activity, i.e., 850% of wild-type (Table 3).

The rrI-titration curve for the reverse reaction is complex, with the concentration of rrI required for half-saturation depending both on the rate of release of the $NADP^+$ formed as well as on the dissociation constant for the rrI·ecIII

Table 3: Rates of the Reverse Reaction Catalyzed by Wild-Type and Mutant ecIII in the Presence of rrI

ecIII enzyme	[ecIII] (nM)	[rrI] (nM)	[rrI]/[ecIII]	V_{max} (mol of AcPyADH) (mol of ecIII)$^{-1}$ min^{-1}	%	ref
ecIII	4900	20	0.004	4	100	*20*
ecIIIH345C	1300	60	0.046	10	250	*20*
ecIIIA348C	690	90	0.130	33	825	*20*
ecIIIR350C	1240	100	0.081	10	250	*20*
ecIIID392C	470	100	0.213	55	1375	*20*
ecIIIT393C	2500	50	0.020	7	175	this study
ecIIIK424C	730	60	0.082	17	425	*20*
ecIIIR425C	1000	90	0.090	17	425	this study
ecIIIG430C	1000	320	0.320	34	850	this study
ecIIIA432C	2500	90	0.036	6	150	this study

[a] The values are estimations derived from rrI−ecIII titration curves where the concentration of rrI was varied (not shown). The assays were carried out in dI·dIII assay buffer (see Materials and Methods). The [ecIII] values refer to the fixed enzyme concentrations used in the protein−protein titrations. The [rrI] values correspond to the concentration of rrI required to reach half-maximal rates.

Table 4: Rates of the Cyclic Reaction Catalyzed by Wild-Type and Mutant ecIII Complexed with rrI[a]

ecIII enzyme	[ecIII] (nM)	[rrI] (nM)	K_d (nM)	V_{max} (mol of AcPyADH) (mol of ecIII)$^{-1}$ min^{-1}	%	ref
ecIII	40	70	50	4900	100	*20*
ecIII	12.5	30	24	4900	100	*20*
ecIII	4	25	23	4900	100	*20*
ecIIIH345C	39	320	300	1250	26	*20*
ecIIIA348C	7	50	46	3300	67	*20*
ecIIIR350C	8	50	46	2000	41	*20*
ecIIID392C	43	450	429	900	18	*20*
ecIIIT393C	12.5	110	104	2400	49	this study
ecIIIK424C	9	60	55	2200	45	*20*
ecIIIR425C	40	60	40	600	12	this study
ecIIIG430C	40	320	300	700	14	this study
ecIIIA432C	12.5	90	84	3100	63	this study

[a] Conditions were as described in Table 3.

complex (*10*). The ratio of rrI/ecIII at $^1/_2V_{max}$ of the reverse reaction was apparently correlated with the rate of reverse transhydrogenation (Table 3), i.e., the release of $NADP^+$. However, the G430C mutant displayed the highest rrI/ecIII ratio even though the activity of the reverse reaction catalyzed by this mutant was not the highest. Obviously, the affinity of the mutant ecIII for rrI was reduced to a greater extent in the G430C mutant than in, e.g., the D392C mutant.

The maximal rate of the cyclic reaction is limited by the hydride transfer steps at pH 7.0 (*10*−*13*). Most ecIII mutants showed relatively high maximal cyclic reaction rates, which indicated an ability of these domains to form catalytically active complexes with rrI similar to wild-type ecIII (Table 4). On the other hand, the most affected mutants, R425C and G430C, showed only 12 and 14% of wild-type ecIII cyclic activity (Table 3), respectively, indicating a substantial loss of hydride transfer ability for these mutants. The corresponding value for D392C was 18%, whereas the remaining mutants showed activities between 26 and 67% of wild-type (Table 4).

The rrI concentration required for half-saturation of the cyclic reaction is a measure of the dissociation constant for the rrI·ecIII complex (*10*). At $^1/_2V_{max}$, 50% of the ecIII molecules take part in complexes with rrI. Depending on the affinity between the two domains, the concentration of rrI required for half-saturation will vary. A K_d for the rrI·ecIII complex is calculated from the actual rrI and ecIII concentrations at $^1/_2V_{max}$, i.e., K_d = [rrI]-[ecIII]/2. The rrI concentration at $^1/_2V_{max}$ was significantly increased in five of the mutants (Table 4). T393C and A432C showed about a 2-fold increase in K_d, whereas the H345C, D392C, and G430C mutants showed a more pronounced increase in K_d, e.g., the G430C mutant displayed more than a 15-fold increase in the concentration of rrI required for $^1/_2V_{max}$. In contrast, despite catalyzing a very low cyclic reaction, R425C displayed an essentially unchanged affinity for rrI as judged by the rrI concentration required for half-saturation of the cyclic reaction (Table 4). This property of R425C is presumably due to its poor ability to bind NADPH in a correct position for hydride transfer (cf. Table 1).

DISCUSSION

Global Fold of ecIII. The solution structure model described in the present investigation defines a distinct global fold and on which side of the β-sheet all α-helices and loops are located. However, at the moment, our NMR data are not sufficient to define the precise positions of all side chains and backbone elements. The loops between β4 and β5 and between β5 and β6 have few structural restraints and it is thus not possible to deduce any detailed structural information for these elements, other than their positions relative to the β-sheet. With these limitations in mind, it is still possible to successfully use the model to interpret the chemical shift perturbations in structural terms.

The NMR solution structure presented in this investigation is quite different from that deduced by NMR of the *R.*

rubrum rrIII (*16*), but very similar to those deduced by X-ray crystallography of bovine mitochondrial (*17*) and human mitochondrial (*18*, *19*) domain III. As a result of the establishment of the crystal structures, a number of residues have been identified as functionally important. The functional roles of the majority of the corresponding *E. coli* residues, most of which are invariant, have previously been characterized extensively using site-directed mutagenesis by Bragg and collaborators (*4*) and by Rydström and collaborators (*3*, *5*, *14*, *20*, *31*).

Substrate Binding and Catalytic Activities. Chemical shift mapping provides general information about the position and extent of the substrate-binding site surface, whereas activity measurements and determination of substrate content of mutant ecIII provides important information regarding the involvement of specific residues in substrate binding. The maximal rate of the reverse reaction catalyzed by the rrI·ecIII complex is limited by the release of $NADP^+$ (*10*−*12*, *32*). V_{max} of the reverse reaction is thus another important indicator for how the NADP(H) affinity has changed due to a mutation of a certain amino acid residue. EcIII mutants with a pronounced increase in the maximal rates of the reverse reaction were A348C, D392C, K424C, R425C, and G430C (Table 3). Chemical shift mapping suggested that these residues were either involved primarily in the ecI−ecIII interface (A348), a redox-regulated interface (A348, D392), or the NADP(H)-binding site (K424, R425, and G430). Taken together, these results thus indicate that all these residues, directly or indirectly, have an important role in substrate binding.

In the recently determined crystal structures of transhydrogenase domain III from bovine (*17*) and human (*19*) heart, details of the NADP(H)-binding site are presented, including hydrogen bonds as well as other interactions between domain III and $NADP^+$. In the crystal structures, A348 is located close to the nicotinamide ring where its carboxyl group is hydrogen bonded to one of the amide protons of $NADP^+$. The carbonyl oxygen of R350 was suggested to take part in electrostatic interactions with the nicotinamide ring (*19*); in addition, the side chain of R350 makes important hydrogen bond contacts with both the ribose moiety of NMN and the pyrophosphate. In the present study, the maximal rate of the reverse reaction catalyzed by the A348C and the R350C mutants was increased by 8 and 2.5 times, respectively, as compared to wild-type ecIII (Table 3). Keeping the positions of A348 and R350 in mind, it is rather surprising that a cysteine mutation in the A348 position caused a more pronounced decrease in $NADP^+$ affinity than in the R350 position. A cysteine residue in the A348 position should be able to in part take over the role of the alanine. In contrast, the side chain of the original arginine in position 350 should be more difficult to replace. This unexpected result suggests that the role of A348 in binding $NADP^+$ is more important in *E. coli* dIII than suggested by the crystal structures.

The pronounced effect of mutating D392 to a cysteine could be explained by its central role in substrate binding (*20*, *31*, *33*), making hydrogen bond contacts both with the ribose moiety of NMN and with the pyrophosphate group (*17*, *19*). The importance of this residue in NADP(H) binding was also demonstrated by the fact that the D392C mutant did not contain any detectable substrate (Table 1). In contrast, the replacement of the nearby T393 by cysteine left the affinity for NADP(H) essentially unaffected. This latter mutant contained bound substrate to 100% and the maximal rate of the reverse reaction was increased only 1.75 times (Tables 1 and 3). Thus, despite being neighboring residues, the side chain of T393 is apparently not involved in NADP(H) binding presumably because it is positioned away from the NADP(H)-binding site.

The remarkable specificity of dIII for NADP(H) relative to NAD(H) (*20*, *34*, *35*) is probably dependent on the interactions between the 2′-phosphate of the nucleotide with the region in the protein composed of K424, R425, and S426 (*17*−*19*). K424−R425−S426 was earlier suggested to play a key role in NADP(H) binding (*5*, *20*, *31*). These conserved amino acid residues are involved in seven proposed hydrogen bonds between NADP(H) and the protein and the side chain of R425 stacks with the adenine (*19*). Mutation of K424 and R425 residues caused dramatic changes in the NADP(H)-binding properties of dIII, the most prominent effect being the lack of bound substrate in the R425C mutant (Table 1). Both K424C and R425C mutants showed a 4-fold increase in the maximal rate of the reverse reaction, reflecting the diminished affinity for $NADP^+$ (Table 3). Interestingly, the R425C mutant was also capable of catalyzing the cyclic reaction in the absence of added $NADP^+$ (C. Johansson, unpublished material), an observation which suggests that this mutant has lost its specificity for NADP(H) without loosing its dinucleotide affinity. The K424R mutant was previously proposed to have lost its low affinity binding of NADH in the cyclic reaction without added NADP(H) (*31*). Taken together, these findings strongly support the original suggestions (*5*, *20*, *31*) that K424 and R425 play a major role in the specificity of dIII for NADP(H).

G430 seems to be of great importance for the mechanism of transhydrogenase for several reasons. This conserved glycine residue allows the close fitting of the dinucleotide-binding motif to NADP(H) and also makes direct contact by its amide group to the ribose of 2′5′-ADP (*17*). The 8-fold increase in the maximal rate of the reverse reaction catalyzed by the G430C mutant may be explained in terms of a lost flexibility caused by the substitution in this position (Table 3). In all mutants discussed above, with the exception of R425C, the $NADP^+$/NADPH ratio was inverted compared to wild-type ecIII, i.e., the proportion of NADPH was increased at the expense of $NADP^+$, the most affected being the G430C and A432C mutants where almost all bound substrate was NADPH (Table 1). It is suggested that this G430−Y431−A432 region constitutes a "redox sensor", which can assume conformations that bind either $NADP^+$ or NADPH. It is extremely interesting that this region also constitutes part of the "lid" suggested to be involved in the occluded state of the enzyme (*18*). It should be stressed, however, that the mechanism by which wild-type ecIII is isolated with mainly bound $NADP^+$, despite the fact that the affinity for NADPH is 2 orders of magnitude higher, is not clear.

Transhydrogenation occurs through direct hydride transfer between the substrates (*36*), i.e., the nicotinamide moieties must be located in near proximity to each other. Many significant chemical shift perturbations occur in the loop connecting β2 and α3, and in α3 itself, upon change of the redox state of NADP(H). In agreement with the available crystal structures of domain III of the bovine and human

enzymes, the distribution of the chemical shift perturbations and the location of the domain interaction surface on ecIII suggest that the nicotinamide moiety in NADP(H) is located near the loop connecting β2 and α3 (residues P346−G353) in ecIII. This conclusion is consistent with the high reactivity of A348C in ecIII with an NADP-analogue with a modified nicotinamide moiety (*20*).

Domain Interactions. The present results, based on chemical shift mapping, clearly indicate that the region which includes residues V319−E328 (α2), G343−E361 (α3 and β3), and G408−V411 form part of the interface between dI and dIII. In addition, residues G389−I406 and G430-V434 are suggested to form a redox-regulated part of the interface. The recently published crystal structures of domain III from human (*19*) and bovine (*17*) transhydrogenase both suggest surfaces of domain III likely to form an interface with domain I. In both cases, the strongly conserved region comprised of residues I344−A362 (the loop connecting β2 and α3, and α3 itself) was proposed to form a rather hydrophobic interface with domain I. The present results confirm that this region indeed is part of the dI·dIII interface (Figure 5A). There were different opinions regarding the role of the conserved acidic region ("acidic patch") formed by residues E361−D383 (from α3 through β3 to α4). This region was proposed to interact either with domain I (*19*) or with the extramembraneous loops of domain II (*17*). In the present NMR experiments these residues were not affected by the addition of ecI, as judged by the observed chemical shift perturbations (Figure 5A), thus excluding the possibility that this region is part of the dI·dIII interface. Other residues that were suggested to form part of an interface with domain I were the conserved G408, M409, and P410 (*17*) and residues involved in nucleotide binding, e.g., Y315, R350, and R425 (*19*). Residues G408−V411 were indeed confirmed to be part of the dI·dIII interface, whereas R350 was confirmed to be part of both the redox-regulated dI·dIII interface and the NADP(H)-binding site. However, Y315 and R425 were not affected upon addition of ecI in the present experiments (Figure 5A), even though they were clearly involved in substrate binding (Figure 5C).

NMR chemical shift mapping has been an excellent tool for determining the interface between domain III and domain I. Activity measurements of the reverse and cyclic reaction catalyzed by mixtures of mutant ecIII and rrI have provided additional information about the involvement of individual residues in the interface, since the effect of a specific mutation in ecIII on the affinity for rrI could be analyzed by rrI−ecIII titrations. In these experiments, the ecIII concentration was kept constant and the rrI concentration was increased until a maximal rate was achieved. The concentration required to reach half-saturation of the cyclic reaction was only dependent on the affinity between the two domains and was thus a measure of the dissociation constant for the rrI·ecIII complex (*10*).

H345, A348, and R350 all form part of the predominately hydrophobic surface proposed to interact with domain I (*17*, *19*). However, of the corresponding cysteine mutants only the H345C mutant displayed a significantly increased amount of rrI required to saturate the cyclic reaction (Table 4). The dissociation constant for the rrI·ecIII complex was unaffected in the A348C and R350C mutants (Table 4). It is therefore unlikely that these latter residues take part in the interaction with domain I directly, even though they are involved in binding to the nicotinamide mononucleotide moiety of NADP(H).

Effect of the Redox State of NAD(P) on Domain Interactions. The D392 has been shown to be surface exposed (*17*) and suggested to play a major role in substrate binding and catalysis (*19*, *20*, *31*, *33*). Mutation of this residue to a cysteine, and also to a lesser degree the T393C mutation, caused a decrease in the affinity for domain I (Table 4), reflecting an apparent involvement in the interface with domain I. The region G389−I406 showed chemical shift perturbations upon reduction of the $NADP^+$ substrate in ecIII (Figure 5C) and it was also identified as an NAD(P)(H) redox-regulated part of the interface with domain I (Figure 5D). This finding is consistent with the proposed key role of D392 in catalytic activity and proton translocation (*20*, *31*, *33*), and may also explain the dramatic changes in the affinity of the *E. coli* (*37*) and bovine heart (*38*, *39*) transhydrogenase for NADH in the presence of an electrochemical proton gradient.

The loop composed of residues G430−V434 was also identified as an NAD(P)(H) redox-regulated part of the interface (Figure 5D). The G430C and A432C mutations were shown to affect the affinity to domain I in the titration of the cyclic reaction (Table 4). In contrast, the K424C and R425C mutants were examples of mutations causing changes in the substrate-binding properties, without affecting the affinity for domain I. The dissociation constant for the complex remained unchanged in both these mutants (Table 4), confirming that neither residue have a role in the interaction with domain I.

A possible mechanism for the above redox-regulated perturbations is that a conformational change, triggered by the replacement of NAD^+ by NADH in ecI, is propagated into ecIII via the concomitant change of $NADP^+$ to NADPH. An alternative mechanism is suggested by the intriguing NAD(H) redox-dependent chemical shift perturbations in β4 (L386, G389), β5 (I421−V422), and β6 (H445−M446) (Figure 5B). According to this mechanism, a conformational change is propagated from NAD(H) into the domain−domain interface, and through α4 reaches the perturbed part of the β-sheet (Figure 5B). It is indeed interesting that this redox-affected region is relatively close to the suggested redox-sensing G430−Y431−A432 region in the C-terminal loop of β5 (see above).

CONCLUSIONS

In this work, a characterization of the interface between domain III and domain I in *E. coli* transhydrogenase has been deduced and an upper limit of the complex lifetime has been estimated. The C-terminal end of the β-sheet forms the substrate-binding site, and the nicotinamide moiety has been confirmed to reside near the loop comprising residues P346−G353. Chemical shift changes in ecIII caused by substrate binding in ecI have been identified and interpreted as a conformational change, possibly important for the reaction mechanism. The loops containing residues G389−I406 and G430−V434 have been identified as involved in a redox-regulated part of the dI·dIII complex interface. It is proposed that these substrate/redox-induced alterations are involved in the reaction mechanism.

ACKNOWLEDGMENT

Dr. Tania Bizouarn is gratefully acknowledged for supplying rrI and for valuable comments on the manuscript, Dr. Tineke Papavoine for assistance in preparing the MOLMOL illustrations, and Dr. Ola Fjellström for valuable discussions. The Swedish NMR Center is acknowledged for measurement time on its NMR spectrometers.

SUPPORTING INFORMATION AVAILABLE

List of chemical shift changes, spanning four pages, between the different complex forms of ecIII as detailed in Figure 5. This material is available free of charge via the Internet at http://pubs.acs.org.

REFERENCES

1. Hatefi, Y., and Yamaguchi, M. (1996) *FASEB J 10*, 444−52.
2. Jackson, J. B. (1999) *Biochim. Biophys. Acta 1365*, 79−86.
3. Rydström, J. (1999) *Biochim. Biophys. Acta 1365*, 10−6.
4. Bragg, P. D. (1999) *Biochim. Biophys. Acta 1365*, 98−104.
5. Fjellström, O., Johansson, C., and Rydström, J. (1997) *Biochemistry 36*, 11331−41.
6. Diggle, C., Hutton, M., Jones, G. R., Thomas, C. M., and Jackson, J. B. (1995) *Eur. J. Biochem. 228*, 719−26.
7. Diggle, C., Bizouarn, T., Cotton, N. P., and Jackson, J. B. (1996) *Eur. J. Biochem. 241*, 162−70.
8. Yamaguchi, M., and Hatefi, Y. (1995) *J. Biol. Chem. 270*, 16653−9.
9. Yamaguchi, M., and Hatefi, Y. (1997) *Biochim. Biophys. Acta 1318*, 225−34.
10. Fjellström, O., Bizouarn, T., Zhang, J. W., Rydström, J., Venning, J. D., and Jackson, J. B. (1999) *Biochemistry 38*, 415−22.
11. Venning, J. D., Bizouarn, T., Cotton, N. P., Quirk, P. G., and Jackson, J. B. (1998) *Eur. J. Biochem. 257*, 202−9.
12. Grimley, R. L., Quirk, P. G., Bizouarn, T., Thomas, C. M., and Jackson, J. B. (1997) *Biochemistry 36*, 14762−70.
13. Bizouarn, T., Grimley, R. L., Cotton, N. P., Stilwell, S. N., Hutton, M., and Jackson, J. B. (1995) *Biochim. Biophys. Acta 1229*, 49−58.
14. Fjellström, O., Olausson, T., Hu, X., Källebring, B., Ahmad, S., Bragg, P. D., and Rydström, J. (1995) *Proteins 21*, 91−104.
15. Johansson, C., Bergkvist, A., Fjellström, O., Rydström, J., and Karlsson, B. G. (1999) *FEBS Lett. 458*, 180−4.
16. Quirk, P. G., Jeeves, M., Cotton, N. P., Smith, J. K., and Jackson, B. J. (1999) *FEBS Lett. 446*, 127−32.
17. Prasad, G. S., Sridhar, V., Yamaguchi, M., Hatefi, Y., and Stout, C. D. (1999) *Nat. Struct. Biol. 6*, 1126−1131.
18. Jackson, J. B., Peake, S. J., and White, S. A. (1999) *FEBS Lett. 464*, 1−8.
19. White, A. W., Peake, S. J., McSweeney, S., Leonard, G., Cotton, N. P. J., and Jackson, J. B. (2000) *Structure 8*, 1−12.
20. Fjellström, O., Axelsson, M., Bizouarn, T., Hu, X., Johansson, C., Meuller, J., and Rydström, J. (1999) *J. Biol. Chem. 274*, 6350−9.
21. Bizouarn, T., Grimley, R., Diggle, C., Thomas, C. M., and Jackson, J. B. (1997) *Biochim. Biophys. Acta 1320*, 265−74.
22. Smith, P. K., Krohn, R. I., Hermanson, G. T., Mallia, A. K., Gartner, F. H., Provenzano, M. D., Fujimoto, E. K., Goeke, N. M., Olson, B. J., and Klenk, D. C. (1985) *Anal. Biochem. 150*, 76−85.
23. Palmer, T., and Jackson, J. B. (1992) *Biochim. Biophys. Acta 1099*, 157−62.
24. Johansson, C., Bergkvist, A., Fjellström, O., Rydström, J., and Karlsson, B. G. (1999) *J. Biomol. NMR 14*, 295−6.
25. Kraulis, P. J. (1989) *J. Magn. Reson. 84*, 627−33.
26. Kraulis, P. J., Domaille, P. J., Campbell Burk, S. L., Van Aken, T., and Laue, E. D. (1994) *Biochemistry 33*, 3515−31.
27. Güntert, P., Mumenthaler, C., and Wüthrich, K. (1997) *J. Mol. Biol. 273*, 283−98.
28. Koradi, R., Billeter, M., and Wüthrich, K. (1996) *J. Mol. Graphics 14*, 51−5, 29−32.
29. Roberts, G. C. K. (1993) *NMR of Macromolecules*, Vol. 134, Oxford University Press, New York.
30. Bizouarn, T., Diggle, C., and Jackson, J. B. (1996) *Eur J. Biochem. 239*, 737−41.
31. Hu, X., Zhang, J., Fjellström, O., Bizouarn, T., and Rydström, J. (1999) *Biochemistry 38*, 1652−8.
32. Peake, S. J., Venning, J. D., and Jackson, J. B. (1999) *Biochim. Biophys. Acta 1411*, 159−69.
33. Meuller, J., Hu, X., Bunthof, C., Olausson, T., and Rydström, J. (1996) *Biochim. Biophys. Acta 1273*, 191−4.
34. Yamaguchi, M., and Hatefi, Y. (1993) *J. Biol. Chem. 268*, 17871−7.
35. Stilwell, S. N., Bizouarn, T., and Jackson, J. B. (1997) *Biochim. Biophys. Acta 1320*, 83−94.
36. Venning, J. D., Grimley, R. L., Bizouarn, T., Cotton, N. P. J., and Jackson, J. B. (1997) *J. Biol. Chem. 272*, 27535−8.
37. Hu, X., Zhang, J., and Rydström, J. (1998) *Biochim. Biophys. Acta 1367*, 134−8.
38. Rydström, J., Da Cruz, A. T., and Ernster, L. (1971) *Eur. J. Biochem. 23*, 212−9.
39. Enander, K., and Rydström, J. (1982) *J. Biol. Chem. 257*, 14760−6.

BI0004091